Supplementary materials to

Optical Absorption, Photocarrier Recombination Dynamics and Terahertz Dielectric Properties of Electron-Irradiated GaSe Crystals

1) The charge carrier relaxation dynamics using the OPTP method and the terahertz photoconductivity were measured using the setup that is shown in Figure S1.

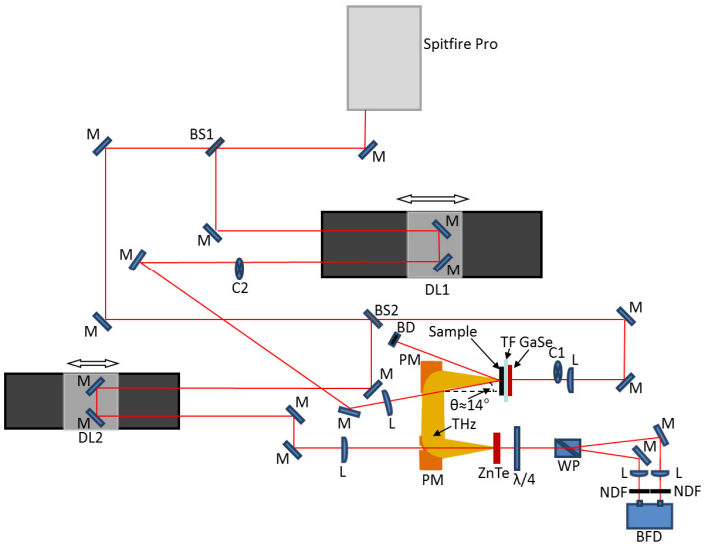

Figure S1. Scheme of the experimental OPTP setup: L—lens, M—mirror, BS1, BS2—beam splitters, DL1, DL2—delay lines, PM—parabolic mirror, TF—Teflon filter, $\lambda/4$—quarterwave plate, WP—Wollaston prism, NDF—neutral density filter, BPD—balanced photodetector, C1, C2—mechanical choppers and BD—beam dump.

For the sample photoexcitation, as well as for the generation and detection of the terahertz pulses, Spitfire Pro XP regenerative amplifier (Spectra-Physics, Milpitas, CA, USA), which generated pulses with a duration of 35 fs and energy up to 3.5 mJ at the central wavelength of 800 nm, was used. The laser pulse from the source, passing through the beam splitting plate (BS1) was divided into two pulses of approximately equal power. One of them, passing the delay line DL1, was used for the sample photoexcitation. The angle of incidence of the photoexcitation pulse θ was about 14° (i.e., the angle between the wavevector and the *c*-axis was about 5° inside the GaSe crystal), and it had vertical polarization (pure ordinary wave). The second pulse was divided using another beam splitter (BS2). The more intense pulse (97% of power) extracted at BS2 passed through an SR-541 chopper (Standford Research, Sunnyvale, CA, USA) and was focused onto a GaSe (served as a detector) crystal to generate a terahertz pulse via optical rectification. Another pulse (3% of power) was directed to the delay line DL2 and then to a ZnTe electro-optical crystal for terahertz pulse detection. With the help of DL2, the simultaneity of the arrival to the ZnTe crystal of the probing optical pulse and the maximum terahertz pulse field strength (the main maximum) transmitted through the sample was established. The signal from the balanced photodetector (BPD) Nirvana Model 2007 (New Focus, Milpitas, CA, USA) was registered using a lock-in amplifier SR-830 (Standford Research, Sunnyvale, CA, USA). The 1D terahertz transmittance scans were made (with DL1), i.e., the temporal profiles of the terahertz pulses were not recorded in the OPTP experiment and only changes in the terahertz pulse field strength at the main maximum were registered.

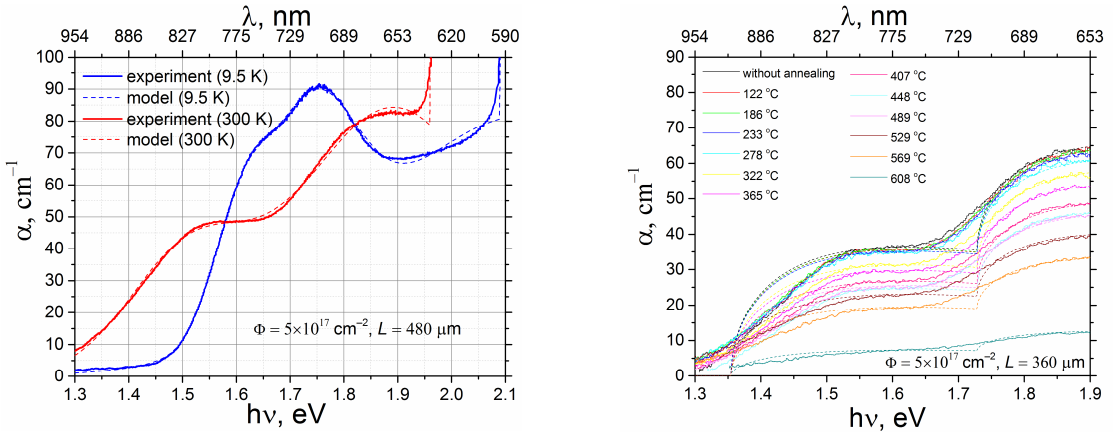

Figure S2. Experimental and fitting (the fitting parameters for Equation (5) in the main text are given in Table S1) optical absorption spectra for the sample $\Phi = 5\times10^{17}$ cm^{-2} measured at temperatures of 9.5 and 300 K (**a**); (**b**) – experimental and fitting (by Equation (4) in the main text) optical absorption spectra for the sample $\Phi = 5\times10^{17}$ cm^{-2} measured at 300 K after isochronal (10 minutes) annealing at different temperatures.

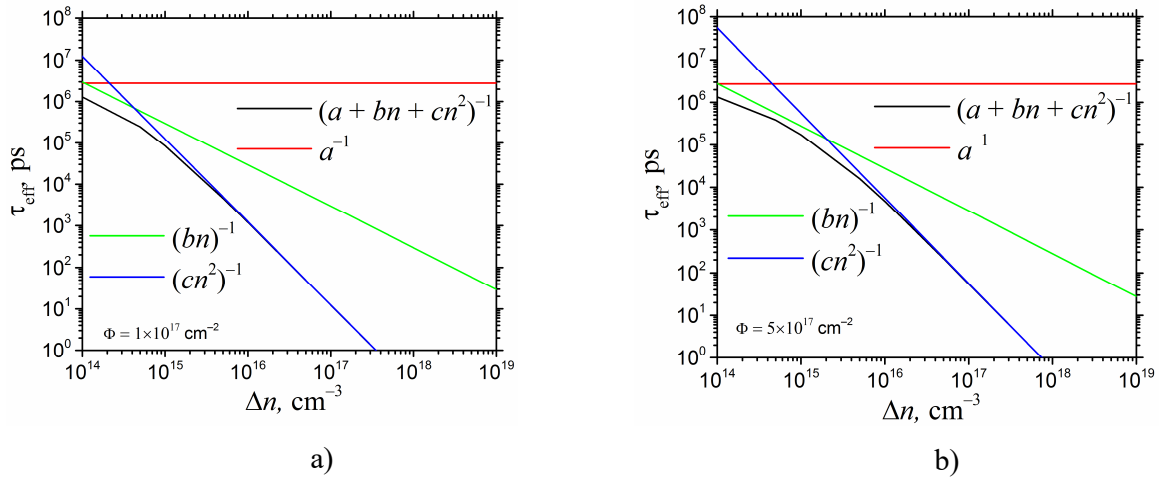

Figure S3. Calculated injection level dependences of efficient charge carrier lifetime with the resolution into contributions from different recombination mechanisms for (a) for the GaSe sample irradiated with fluence of 1×10^{17} cm^{-2} and (b) for the GaSe sample irradiated with fluence of 5×10^{17} cm^{-2}.

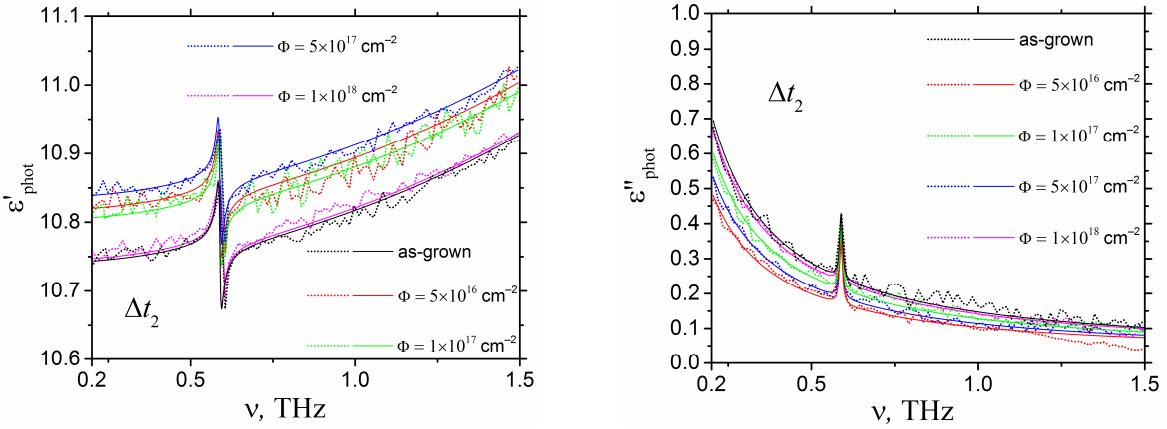

Figure S4. The terahertz spectra of real (**a**) and imaginary (**b**) parts of complex dielectric constant measured in as-grown and electron-irradiated GaSe crystals at a time delay Δt_2 after photoexcitation. Dotted lines – experimental data, solid lines –Lorentz–Drude–Smith fitting (the fitting parameters are given in Table 4 in the main text).

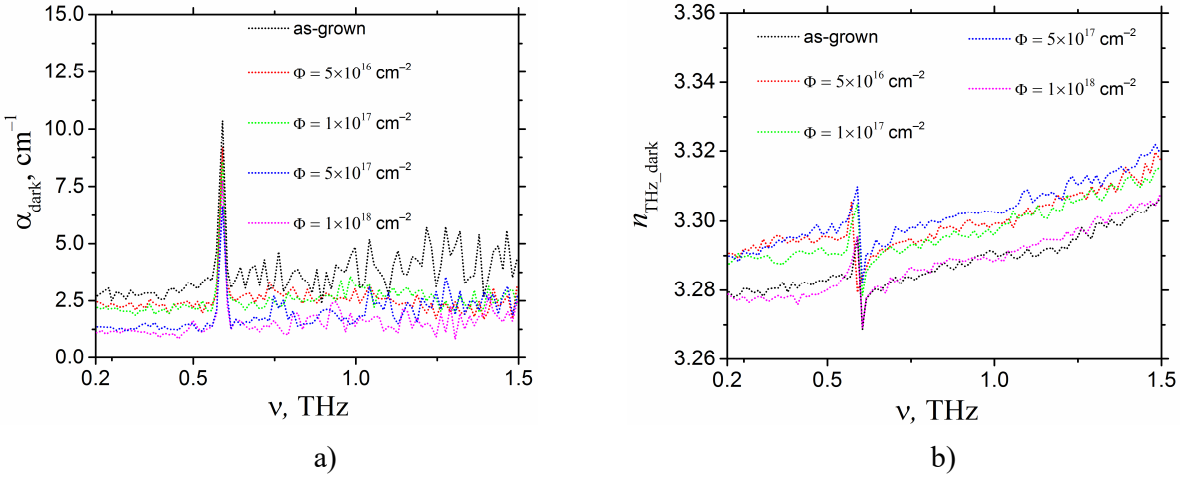

Figure S5. The terahertz spectra of the absorption coefficient (**a**) and ordinary refractive index (**b**) measured in as-grown and electron-irradiated GaSe crystals (without photoexcitation).

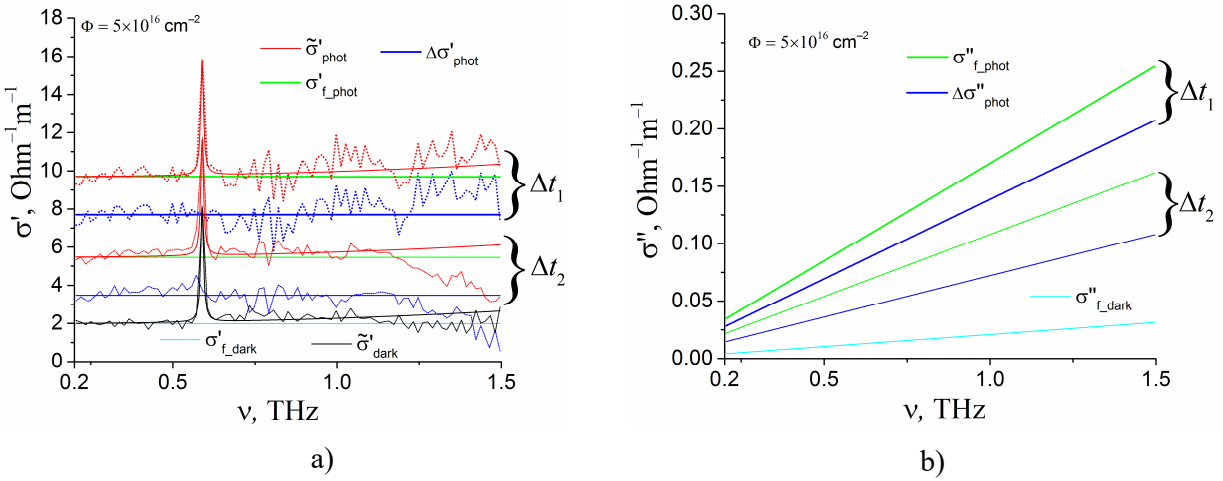

Figure S6. The terahertz spectra of real parts of the total conductivity, photoconductivity and free carrier conductivity (**a**) and imaginary parts of photoconductivity and free carrier conductivity (**b**) measured in the dark and at delays Δt_1 and Δt_2 after photoexcitation for the irradiated with fluence $\Phi = 5\times10^{16}$ cm^{-2} GaSe sample. |Dotted lines – experimental data, solid lines – Lorentz–Drude–Smith fitting (the parameters are given in Table 4 in the main text).

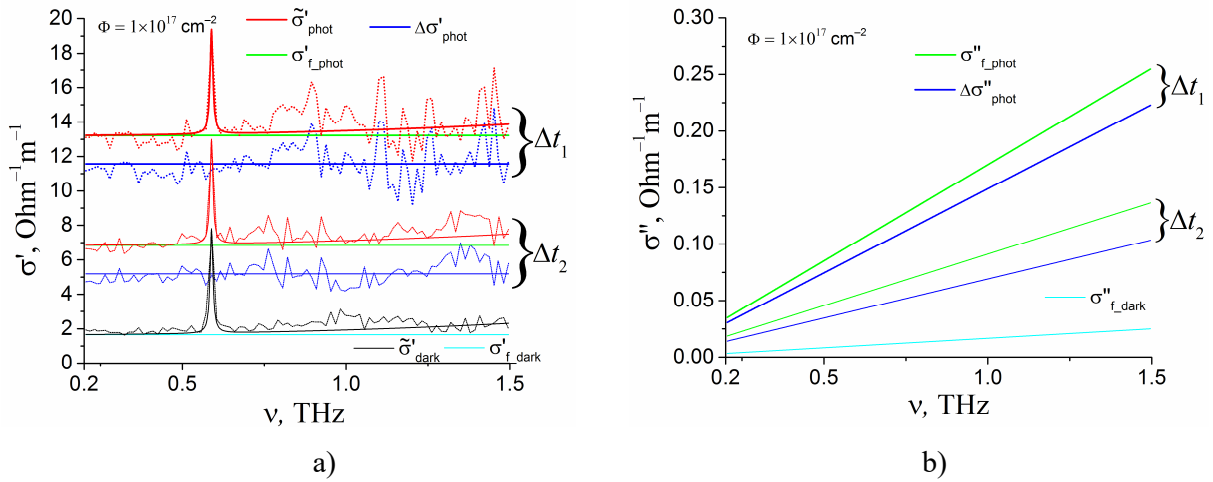

Figure S7. The terahertz spectra of real parts of the total conductivity, photoconductivity and free carrier conductivity (**a**) and imaginary parts of photoconductivity and free carrier conductivity (**b**) measured in the dark and at delays Δt_1 and Δt_2 after photoexcitation for the irradiated with fluence $\Phi = 1\times10^{17}$ cm^{-2} GaSe sample. Dotted lines – experimental data, solid lines – Lorentz–Drude–Smith fitting (the parameters are given in Table 4 in the main text).

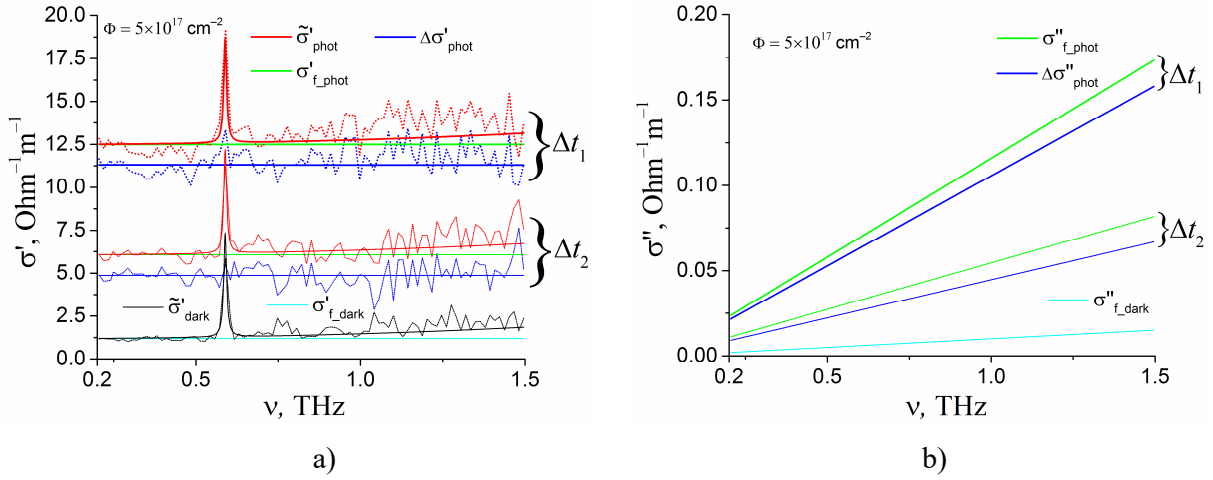

Figure S8. The terahertz spectra of real parts of the total conductivity, photoconductivity and free carrier conductivity (**a**) and imaginary parts of photoconductivity and free carrier conductivity (**b**) measured in the dark and at delays Δt_1 and Δt_2 after photoexcitation for the irradiated with fluence $\Phi = 5\times10^{17}$ cm^{-2} GaSe sample. Dotted lines – experimental data, solid lines – Lorentz–Drude–Smith fitting (the parameters are given in Table 4 in the main text).

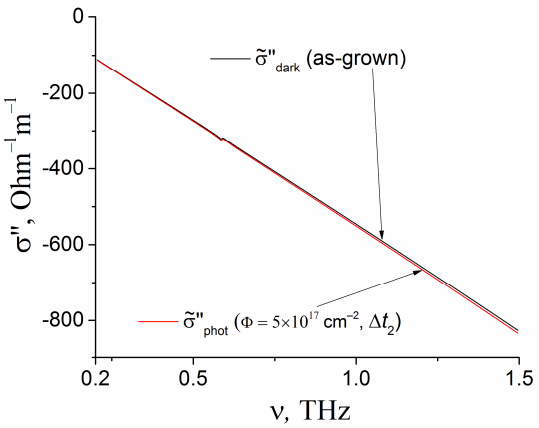

Figure S9. The model terahertz spectra of imaginary parts of dark total conductivity for the as-grown GaSe sample and total conductivity for the GaSe sample irradiated with fluence $\Phi = 5\times10^{17}$ cm^{-2} for the delay Δt_2 after photoexcitation (the fitting parameters are given in Table 4 in the main text). The curves for of imaginary part total conductivity of the other samples and measured at other photoexcitation conditions are not plotted because they are very close to the shown ones.

Table S1. The fitting parameters obtained during fitting with Equation (5) (in the main text) of the optical absorption spectra for the sample $\Phi = 5\times10^{17}$ cm^{-2} measured at temperatures of 9.5 and 300 K.

Parameter	9.5 K	300 K
B_1, cm^{-1}	30.17283	35.53749
c_1, eV^2	1.60484	1.50997
E_1, eV	0.00519	0.02543
B_2, cm^{-1}	57.83449	84.2317
c_2, eV^2	1.73616	1.89349
E_2, eV	0.01436	0.06547
B_3, cm^{-1}	81.52847	-
c_3, eV^2	2.13179	-
E_3, eV	0.15817	-
B_4, cm^{-1}eV$^{-1/2}$	1947	1947
E_g, eV	2.09	1.96

2) The A_3 parameter in Equation (4) in the main text was calculated (and kept fixed during fittings) for GaSe employing a well-known formula (see, for example, Ref. 46 in the main text)

$$A = \frac{e^2\left(2\frac{m_e^* m_h^*}{m_e^* + m_h^*}\right)^{3/2}}{nch^2 m_e^*} \times \sqrt{1.6\cdot10^{-12}}\,\text{eV}^{-1/2}\text{cm}^{-1}$$

where the values must be substituted in CGS system of units. The following values were used $m^*_e = 0.17m_0$, $m^*_p = 0.8\,m_0$, (Ref. 44 in the main text), n=2.95.

3) When calculating concentrations of defects N in each of V_{Ga}^{-1} and V_{Ga}^{-2} charge states we used the following Gibbs distribution functions (see, for example, Ref. 46 in the main text), taking into

account that the multiple charge states produce higher energy states only when the lower state is occupied and the lower occupied state can't be optically active if the higher state is occupied:

$$f1 = M\exp(\frac{E_{\mathrm{f}} - E_{\mathrm{g}} + E_{\mathrm{A2}}}{kT})$$

for the V_{Ga}^{-1} state and

$$f2 = M\exp(\frac{2E_{\mathrm{f}} - 2E_{\mathrm{g}} + E_{\mathrm{A1}} + E_{\mathrm{A2}}}{kT})$$

for the V_{Ga}^{-2} state, where

$$M = \frac{1}{\exp(\frac{E_{\mathrm{f}} - E_{\mathrm{g}} + E_{\mathrm{A2}}}{kT}) + \exp(\frac{2E_{\mathrm{f}} - 2E_{\mathrm{g}} + E_{\mathrm{A1}} + E_{\mathrm{A2}}}{kT}) + 1}.$$

We assumed the simplified case when the defect can be only in three possible charge states (j = 0, –1, –2) and in each charge state there is no excited energy states and degeneracy. The zero-energy level is at VBM. Thus the defect center energy increase when the electron occupies the neutral acceptor defect is E_g–E_{A2} and the defect center energy increase is E_g–E_{A1} when the electron occupies the V_{Ga}^{-1} defect. The E_{A1} and E_{A2} are the optical transition energies and E_g is the band gap (see Table 2 in the main text).

The following formula in CGS system of units was used to find N values (j = 1, 2):

$$A_{\mathrm{j}} = \frac{N}{n(\hbar\omega = E_{\mathrm{Aj}})}\left(\frac{E_{\mathrm{eff}}}{E_0}\right)^2 \frac{16\pi e^2 \hbar E_{\mathrm{Aj}}^{3/2}}{3m^* c} \approx 2.19\cdot 10^{-15} \times \frac{N\cdot E_{\mathrm{Aj}}^{3/2}}{n(\hbar\omega = E_{\mathrm{Aj}})}\,\mathrm{cm}^{-1}\mathrm{eV}^{5/2}$$

if m^* = 0.17m_0, (E_{eff}/ E_0)=2. Thus, substituting to this equation E_{A1} and E_{A2} values from Table 2 in the main text and related values of refractive index n (2.84 and 2.81 for E_{A1} at 9.5 and 300 K, respectively; 2.87 and 2.88 for E_{A2} at 9.5 and 300 K, respectively), the value of N was fitted to match A_j value from Table 2 in the main text.